COMMUNICATION

Check for updates

In(III)-dictated formation of double Cs$_2$Ag$_x$Na$_{1-x}$Fe$_y$In$_{1-y}$Cl$_6$ perovskites†

Oleksandr Stroyuk, [image: ORCID] *[a] Oleksandra Raievska,[a] Anastasia Barabash,[b] Jens Hauch[ab] and Christoph J. Brabec[ab]

Stable double Cs$_2$Ag$_x$Na$_{1-x}$Fe$_y$In$_{1-y}$Cl$_6$ (CANFIC) microcrystalline perovskites were produced in air-open conditions. In(III) was found to steer the precursor interaction exclusively towards single-phase solid-solution CANFIC perovskite microcrystals with well-controlled composition, even when present at a small amount (1%). CANFICs revealed sensitivity in the visible range with the lowest bandgap of 1.95 eV found for $y = 0.99$. Due to a combination of open-environment synthesis conditions, reliable compositional control, the abundant and relatively non-toxic character of constituents, stability, and absorbance in the visible spectral range, CANFIC perovskites show high promises for photovoltaic and photochemical applications.

Double metal halide perovskites A$_2^I$M^{I}M^{III}X$_6$ (A^I – alkali metal or organic cation, M^I and M^{III} – metal cations, X – halide anion) offer unrivaled variability of composition, allowing versatile substitutions on each of the four key positions – A^I, M^I, M^{III}, and X, at the same time retaining unique electronic properties of the perovskite lattice.[1–4] Double chloride perovskites with large bandgaps (2–3 eV) often exhibit very efficient broadband photoluminescence (PL) originating from self-trapped excitonic states with PL quantum yields reaching ultimate values of 90–100%.[3–5] Double bromide and iodide perovskites sensitive to visible and near-infrared light show high promises for applications in photovoltaics, in particular as components of tandem solar cells[6–10] as well as in photocatalysis.[11] At the same time, bromide and iodide double perovskites are often prone to oxidation and decomposition resulting in high demand for much more stable chloride perovskites with narrow bandgaps.

For a given halide X, the electronic and optical properties of a double perovskite can be strongly affected by alloying two (and

possibly more) metals on both M^I and M^{III} positions,[4,8] typical examples being the combinations of Ag$^+$ with Na$^+$ on M^I sites and In^{3+} with Bi^{3+} or Sb^{3+} on M^{III} sites.[3,4] At that, the introduction of a second metal into M^I and M^{III} positions can lead to dramatic changes in the spectral sensitivity range, charge transport properties, PL efficiency, *etc.*, even at very small amounts of the second metal additive. This phenomenon is vividly illustrated by Cs$_2$Ag$_x$Na$_{1-x}$InCl$_6$ (abbreviated as CANIC by the first letters of constituent elements) perovskites, showing an enormous boost of PL quantum yield up to 100% and a strong bandgap narrowing after the substitution of merely 1% of In^{3+} with Bi^{3+}.[3,5,12]

The potential of design of the properties of double halide perovskites through M^I/M^{III} substitutions stimulated a search for new "guest" cations for "host" perovskite matrices, for example, rare-earth cations to obtain new luminescent materials[3,5] or earth-abundant Fe^{3+} cations to shift the spectral sensitivity to the visible and near-infrared range.[6] The latter approach was marked by recent reports on Cs$_2$NaFeCl$_6$,[13] Cs$_2$Ag$_x$Na$_{1-x}$FeCl$_6$,[14,15] Cs$_2$AgFe$_y$In$_{1-y}$Cl$_6$,[16,17] and Cs$_2$NaFe$_y$Bi$_{1-y}$Cl$_6$ perovskites[18] showing spectral sensitivity down to 800 nm and promising charge transport properties. These reports, however, were focused on the hydrothermal synthesis of perovskite single crystals, which is highly energy-intensive and offers limited scalability and control over the perovskite composition.

In the present communication, an alternative approach is developed for an open-environment, reproducible, and scalable synthesis of microcrystalline Cs$_2$Ag$_x$Na$_{1-x}$Fe$_y$In$_{1-y}$Cl$_6$ CANFIC perovskites with controlled composition. This synthesis is based on perovskite precipitation from acidic aqueous solutions and exploits a unique capability of very small additions of In^{III} to drive the precipitation exclusively toward the spontaneous formation of a CANFIC perovskite phase as a single product.

Double CANFIC perovskites were synthesized *via* precipitation from highly acidic aqueous solutions at room temperature (RT) and in an air-open atmosphere. To steer the precipitation towards the formation of CANFIC perovskite as a single phase,

^{a} Forschungszentrum Jülich GmbH, Helmholtz-Institut Erlangen Nürnberg für Erneuerbare Energien (HI ERN), 91058 Erlangen, Germany
E-mail: o.stroyuk@fz-juelich.de

^{b} Friedrich-Alexander-Universität Erlangen-Nürnberg, Materials for Electronics and Energy Technology (i-MEET), Martensstrasse 7, 91058 Erlangen, Germany

† Electronic supplementary information (ESI) available. See DOI: https://doi.org/10.1039/d3tc01138k

This journal is © The Royal Society of Chemistry 2023

J. Mater. Chem. C, 2023, 11, 6867–6873 | 6867

the constituent M^{3+} cations (Fe, In) and M^+ cations (Cs, Ag, and Na) were separated into two precursors, thus minimizing any possible side reactions between M^+ and M^{3+} in the precursors. The composition of each of the two precursor solutions was also tuned to avoid side hydrolytic processes. In particular, the M^{3+}-precursor #1 was prepared in concentrated (12 M) HCl, while the hydrolysis of Ag^+ in the alkaline medium created by Cs and Na acetates in the aqueous M^+-precursor #2 was suppressed by binding Ag^+ in an ammonia complex with NH_4OH. No additional thermal treatment was applied to the as-precipitated CANFIC products.

The composition of both precursors was optimized to achieve the formation of CANFIC perovskite of a given composition as a single and stable phase. The optimization included a variation of the Cs/(Fe + In) ratio, as well as concentrations of HCl and NH_4OH using phase-purity shown by XRD as a performance indicator (more details provided below).

In the optimized synthetic procedure the nominal Fe-to-In ratio y was varied by introducing different amounts of $FeCl_3$ and $InCl_3$ to precursor #1, while precursor #2 contained constant amounts of $AgNO_3$ and NaAc.

In this way, precursor #1 was prepared by adding y μL of 1.0 M aqueous $FeCl_3$ solution and $(100 - y)$ μL of aqueous $InCl_3$ solution to 600 μL of concentrated (12 M) aqueous HCl solution. Precursor #2 was prepared by adding to 100 μL of aqueous 1 M $AgNO_3$ solution consecutively and under intense stirring 30 μL of concentrated aqueous 14 M NH_4OH solution, 25 μL of aqueous 4 M NaAc solution, and 100 μL of aqueous 4 M CsAc solution.

The presence of excessive cesium and sodium chlorides over stoichiometric amounts is a necessary condition for the formation of pure perovskite CANFIC phases. In separate series with varied Ag-to-Na ratios, precursor #2 was prepared either with different amounts of $AgNO_3$ at a constant NaAc content or with different amounts of NaAc at a constant $AgNO_3$ content. At that, the constant amounts of NaAc or $AgNO_3$ were taken according to the CANFIC stoichiometry.

The precursors were rapidly mixed under intense stirring at RT by adding precursor #2 to precursor #1, resulting in the precipitation of CANFIC products. The as-precipitated CANFIC suspensions were left in a closed vial for 12–15 h with no stirring to achieve deeper CANFIC crystallization. The supernatant solutions were separated, and 1.0 mL of 2-propanol was added to each vial to remove unreacted residuals of precursors. The mixture was subjected to centrifugation at 3000 rpm, the precipitate separated, and the purification procedure was repeated once more. Final powders were dried at RT and relative humidity of 50–60% and kept in the dark under ambient conditions.

Additional details on the preparation of an exemplary CANFIC sample with 5% In as well as on the instruments and methods used can be found in ESI.†

The presented protocol yields 50 mg of CANFIC perovskites, corresponding to a mass product yield of 83%. The proposed synthetic approach is readily scalable for the production of gram quantities of CANFIC perovskites, with the mass product yield remaining constant with the volumes of reactants multiplied by factors of 10 and 20. A repeated inspection of the structure and spectral characteristics of CANFICs produced in different batches and scales of the synthesis (from mg to g) showed very good reproducibility of the properties of final products.
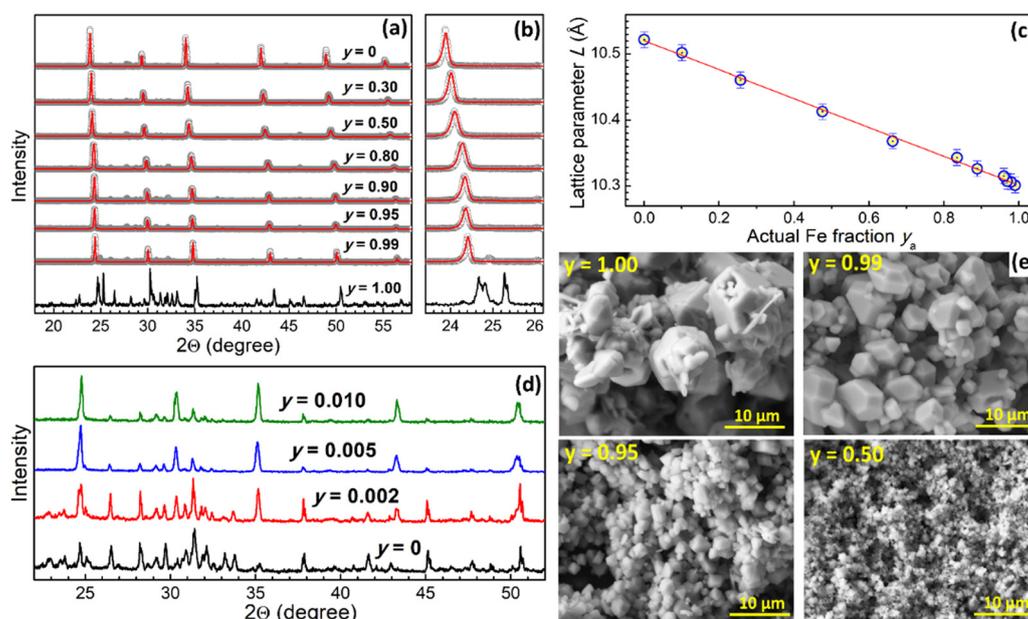
Fig. 1 (a, b and d) XRD patterns of CANFIC products synthesized at higher (a and b) and lower (d) nominal Fe/(In + Fe) ratios y. Figure (b) is a close-up of (a) at lower angles. In (a and b) gray scatter represents experimental data, solid line – results of Rietveld refinement. (c) Lattice parameter L of CANFICs as a function of the actual Fe fraction y_a (scatter), solid line represents a linear fit $L = 10.522 - 0.219y_a$, coefficient of determination $R^2 = 0.998$. (e) SEM images of CANFIC products synthesized at different y.

6868 | *J. Mater. Chem. C*, 2023, **11**, 6867–6873

This journal is © The Royal Society of Chemistry 2023

Structure, composition, and morphology of CANFIC perovskites

Iron-free $Cs_2Ag_xNa_{1-x}InCl_6$ (CANIC) compound produced at nominal $x = 0.50$ shows a typical perovskite XRD pattern (Fig. 1a, scatter 1) corresponding to the cubic $Fm\overline{3}m$ structure,[3,12,16–20] Rietveld refinement of the pattern (solid line 1) showing no additional phases and yielding a lattice parameter $L = 10.522$ Å (Fig. 1d).

Gradual substitution of In(III) with Fe(III) results in a gradual shift of the XRD peaks to higher degrees (Fig. 1a and b) indicating lattice contraction without any change of the lattice structure and formation of new phases almost in the entire range of molar Fe-to-In ratios ($y = 0$–0.99). The reduction of the lattice parameter reflects the fact that the Fe^{3+} cation has a smaller radius (64 Å) as compared to In^{3+} (81 Å).[16]

A gradual lattice transformation (Fig. 1a and b) and a linear decrease of the lattice parameter of CANFIC compounds is observed as y is elevated from 0 up to 0.99 (Fig. 1c), indicating the formation of solid-solution compounds in the entire studied range of Fe-to-In ratios. It should be noted that the variation of Fe-to-In ratio in such a broad range is, to the best of our knowledge, reported for the first time, although the feasibility of the incorporation of moderate amounts of Fe^{3+} (10%) into double Bi, In, and Sb chloride perovskites was documented.[16]

However, no perovskite was detected by XRD when only Fe(III) is introduced into the precursors, the products showing a different XRD pattern (Fig. 1a and b, $y = 1.00$). In this case, the precipitation results in a brown-orange amorphous product transforming after 48 h of crystallization into burgundy-colored crystals, which are stable only under 2-propanol and show rapid hydrolytic degradation when exposed to environmental moisture with relative humidity higher than ca. 50%.

The striking difference between the structures of pure Cs–Ag–Na–Fe–Cl (CANFC) product and CANFIC perovskite with merely 1% of In (Fig. 1a and b, $y = 0.99$) shows that this tiny In(III) admixture acts as a structure-directing factor, which guides the entire system exclusively to the formation of pure CANFIC perovskite phase. This effect of In(III) was tracked by varying the nominal Fe fraction y between 1.00 and 0.99 (Fig. 1d). The formation of CANFIC perovskite among other phases was detected in XRD patterns even at 0.2% In (curve 2 in Fig. 1d). At 0.5% In CANFIC is observed as a major phase (curve 3), while at 1% In CANFIC becomes the exclusive product of the synthesis (curve 4).

Similar to the crystal structure, the morphology of CANFIC compounds showed a profound transformation as an admixture of 1% In is introduced to the CANFC system, and then the Fe fraction is gradually reduced to zero. SEM inspection showed the CANFC microcrystals to be polydisperse both in shape, showing the presence of large polygons as well as needle-like and platelet crystals, and in size, the latter varying from below 1 μm to ca. 10 μm (Fig. 1e, $y = 1.00$). The introduction of 1% In directs the system to the formation of well-faceted polygons with sizes from 2 to ca. 7–8 μm (Fig. 1e, $y = 0.99$). Further increase in the In content results in a gradual decrease of the polygon size down to 1–2 μm at $y = 0.50$ (Fig. 1e, $y = 0.50$), while no noticeable evolution of the CANFIC morphology can be observed at $y < 0.50$ (Fig. S1, ESI†).

Along with In(III), the simultaneous presence of both Ag(I) and Na(I) was found to be crucial for the formation of CANFIC perovskites. Pure perovskite polygonal microcrystals were produced only from the precursors containing In, Ag, and Na together, while the exclusion of either In, Ag, or Na, or both Ag and Na resulted in mixed-phased products with complex XRD patterns and irregular crystal shapes (ESI,† Fig. S2). As a result, the proposed approach cannot produce purely Ag-containing or purely Na-containing perovskites as single-phase products.

The actual composition of CANFIC perovskites with varied x and y ratios was tested by EDX analysis after triple purification of the products from residual salts as described above. The compositions of studied compounds are summarized in ESI† (Table S1).

The actual Fe fraction y_a was found to be in very good agreement with the nominal Fe fraction y (set at the synthesis via the precursor ratio). The relation between y_a and y is linear
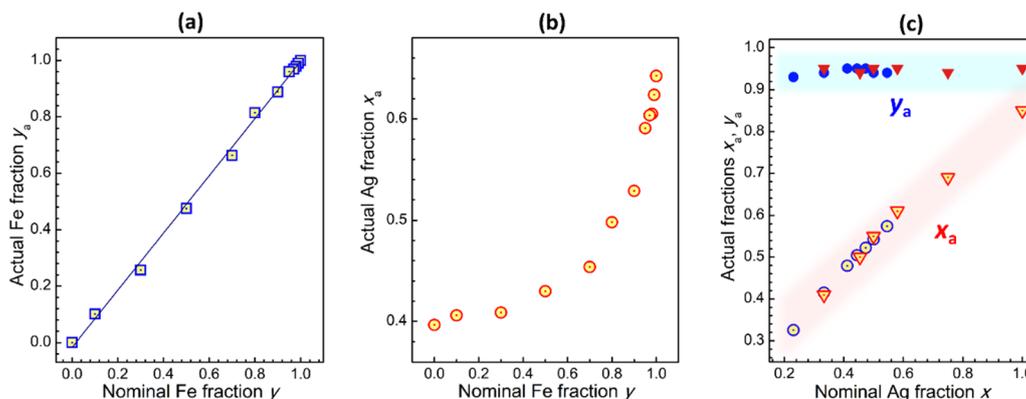
Fig. 2 (a and b) Actual molar fractions of iron y_a (a) and silver x_a (b) as functions of the nominal Fe fraction y. The solid line in (a) represents the linear fit of scatter 1 (slope is 1.01, coefficient of determination $R^2 = 0.998$). In (a and b) nominal $x = 0.50$ with 100% excess of Ag^+ and Na^+ over the formal stoichiometry for all samples. (c) Actual molar Ag and Fe fractions as functions of the nominal Ag fraction x. Scatters represented by circles were collected by varying Ag content at a constant Na content, triangle scatters – by varying Na content at a constant Ag content.

in the entire probed range with a slope of almost unity (Fig. 2a and Table S1, ESI†), showing a reliable control over the Fe-to-In ratio. At the same time, the actual Ag-to-Na ratio x_a deviates from the nominal x depending on the Fe content. The CANFIC compounds with higher Fe content were found to be enriched with silver, while the perovskites with lower Fe content – with sodium (Fig. 2b and Table S1, ESI†). The Cs and Cl contents were found to be close to the stoichiometric values of Cs/(Fe + In) = 2 and Cl/(Fe + In) = 6 for all studied compounds. We note also that the latter value showed an insignificant but steady trend of increasing from ca. 5.3 to ca. 6.2 as the Fe fraction y was elevated from 0.10 to 0.99 (ESI,† Table S1). In every case, a 200% excess of CsCl over the stoichiometric value was found to be needed to reach deeper crystallization and more complete precipitation of CANFIC perovskites.

The synthesis of CANFIC compounds developed here is performed at RT and air-open environment, allowing the most thermodynamically stable product to form for each particular precursor composition. For each sample with varied y equal amounts of Ag^+ and Na^+ were introduced ($x = 0.50$) with both cations taken in 100% excess over the formal stoichiometry. As discussed above, the presence of excessive Cs^+, Ag^+, and Na^+ is required for the formation of pure CANFIC phases. Unreacted Cs^+, Na^+, and Ag^+ salts were removed with the supernatants after the CANFIC precipitation due to the good solubility of corresponding chlorides in concentrated HCl.

Most probably, each Fe-to-In ratio in CANFIC is related to a specific "preferable" Ag-to-Na ratio and, for this reason, the variation of y cannot be uncoupled from the spontaneous variation of x. The In-richer CANFIC lattice shows a preference for incorporating Na cations, while the Fe-richer lattice – Ag cations. The possible formation of the AgCl phase as a reason for the increased Ag and Cl content for Fe-richer compounds was dismissed based on the phase purity of CANFIC products revealed by XRD. No AgCl-related reflections were detected indicating that AgCl, even if present, is below 5 mass% of the products.

At the same time, a variation of Ag-to-Na ratio x at a constant y was found to be a feasible way of changing the relative Ag content without affecting the actual Fe-to-In ratio. Two approaches were tested, particularly by changing Ag content on the background of a constant Na content and, vice versa, by varying Na content at a constant Ag content. XRD study of the products in both series (ESI,† Fig. S3) showed that CANFICs retain cubic perovskite structure in the range of 0.1–0.2 < x < 0.6–0.7. As discussed above, no CANFIC perovskite is formed in the absence of Ag, Na, or Ag + Na, while additional phases can be detected at $x > 0.60$. The morphology of CANFIC produced at varied x was also found to be the same, provided that the Ag-to-Na ratio falls in the range of 0.1–0.2 < x < 0.6–0.7 (ESI,† Fig. S4).

Both approaches to the x variation found to yield similar results (Fig. 2c). The relations between the actual Ag-to-Na ratio x_a and nominal x were close to linear ones and overlapped for both series of samples (open circles and triangles in Fig. 2c), yielding a general $x_a(x)$ dependence. At that, the Fe-to-In ratio was found to be almost constant for all tested cases (filled circles and triangles in Fig. 2c).

We note also that the inadvertent variation of the Ag-to-Na ratio at a constant y does not contribute significantly to the lattice parameter of CANFIC perovskites (ESI,† Fig. S5), allowing the linear relation between the lattice parameter and the actual Fe fraction y_a to be clearly observed (Fig. 1c, ESI†), despite simultaneous changes in both y_a and x_a (ESI,† Table S1).

In summary, both Fe-to-In and Ag-to-Na ratios can be varied simultaneously for any particular composition of CANFIC perovskite. This variability can become crucial for applications of CANFIC perovskites in PV and photocatalysis because the variations of both Fe-to-In and Ag-to-Na ratios affect strongly the absolute positions of conduction/valence bands,[14,16] electron mobility,[14] as well as the charge carrier diffusion length[14] in these perovskites.

Along with the two most important parameters, x and y ratios, other possible variables of the CANFIC synthesis were also varied in reasonable ranges. These variables include the Cs/(Fe + In) ratio, the amount of concentrated HCl introduced to the precursors, and the amount of NH_4OH used to bind Ag^+ and avoid by-side hydrolytic processes in precursor #2. The CANFICs yielded from these variations were examined by XRD (ESI,† Fig. S6), and reaching the CANFIC perovskite phase purity was accepted as a selection criterion. The optimization of the synthesis resulted in a general synthetic protocol presented above.

Spectral properties of CANFIC perovskites

Spectral characterization of CANFIC perovskites included an analysis of the off-resonance Raman and UV-Vis absorption spectra depending on the parameters x and y. The CANFICs were found to be non-luminescent materials, at least at the conditions of spectral experiments (RT, open-air atmosphere, excitation at 280–370 nm).

Iron-free CANIC perovskite shows two major Raman peaks at 293.5 cm^{-1} and 139.5 cm^{-1} (Fig. 3a, $y = 0$), assigned to A_{1g} and T_{2g} vibrational modes of $[InCl_6]^{3-}$ octahedra.[3,12,19,20] Incorporation of Fe(III) into the perovskite results in a series of distinct spectral changes, including a general decrease of the scattering intensity, a considerable broadening and a shift of the A_{1g} band to lower frequencies, gradual extinction of the T_{2g} feature and formation of a new broader band at 158 cm^{-1} (Fig. 3a). Among these changes, the A_{1g} band shows the most distinct and continuous evolution depending on the nominal Fe fraction y.

In particular, the A_{1g} frequency gradually falls from 293.5 cm^{-1} for pure CANIC to 285.2 cm^{-1} for CANFIC as the Fe-to-In ratio is increased from zero to 0.99 (scatter 1 in Fig. 3b). This position is still quite different from the A_{1g} band frequency reported for $[FeCl_6]^{3-}$ octahedra in pure CNFC and CANFC single crystals, 294–302 cm^{-1},[15,21,22] indicating a strong effect of In^{III} addition on the lattice dynamics, even at the indium content being as small as 1%.

6870 | J. Mater. Chem. C, 2023, 11, 6867–6873

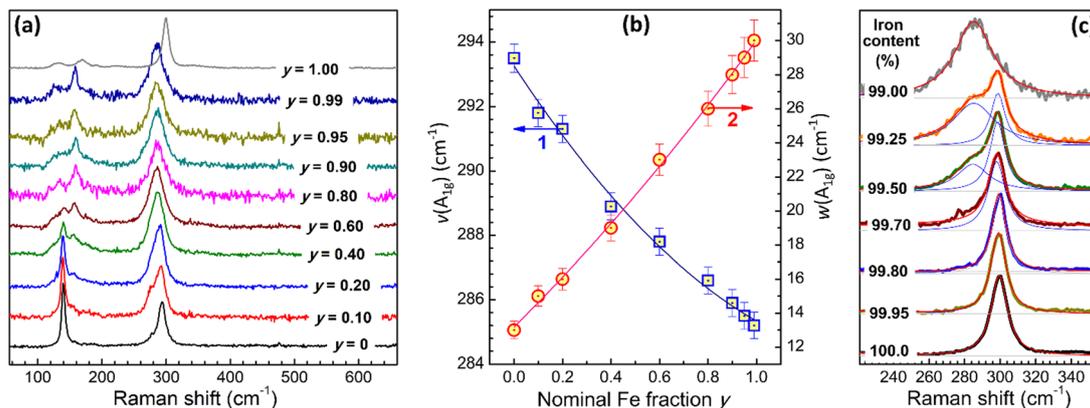This journal is © The Royal Society of Chemistry 2023

Fig. 3 (a and c) Raman spectra of CANFIC perovskites produced at varied nominal Fe content y. In (c): red and blue lines show a multi-Lorentzian fitting of the spectra. (b) Peak frequency $v(A_{1g})$ (scatter 1) and spectral width $w(A_{1g})$ of the A_{1g} band (scatter 2) of CANBIC perovskites as functions of the nominal Fe content y. Solid lines represent polynomial fits of the scatters, $v(A_{1g}) = 293.3 - 0.12y + 0.0004y^2$ ($R^2 = 0.992$), $w(A_{1g}) = 13.2 + 0.14y + 2.77y^2$ ($R^2 = 0.998$).

Simultaneously with the shift, the A_{1g} band shows a considerable broadening, the spectral width growing from 13 cm^{-1} for CANIC to 30 cm^{-1} for CANFIC with 99% Fe (scatter 2 in Fig. 3b). The broadening of the A_{1g} band as well as suppression of the Raman scattering with increased y most probably reflect disordering of the CANFIC lattice due to the Fe–In mixing. A considerable disorder is probably an inherent feature of Fe-based double compounds, reflecting, for example, in a unique disorder-governed thermochromic behavior of CNFC single crystals.[13] An indirect indication of a high lattice disorder in CANFIC compounds can be the absence of PL emission, observed for CAFIC single crystals.[16] The dependences of the A_{1g} frequency and the A_{1g} bandwidth can be fitted by second-order polynomial functions (see solid lines and legend in Fig. 3b), both useful for the identification of the CANFIC composition purely from spectral data.

In agreement with the XRD data Raman spectrum of pure CANFC product (Fig. 3a, $y = 1.00$) was found to be distinctly different from the spectra of both CANIC and CANFIC perovskites. Similar to XRD, Raman spectroscopy was found to be sensitive enough to track the evolution from pure CANFC to CANFIC with 1% In through a series of samples with very low indium contents. The most prominent Raman band of pure CANFC at 299.9 cm^{-1} can be fitted with a single Lorentzian profile (Fig. 3c, $y = 1.00$). Introduction of indium results in the formation of a second band, already clearly visible for the sample with 0.50% In and peaked at *ca.* 285 cm^{-1} (Fig. 3c, 99.5% Fe). This peak becomes much more intense for 0.75% In and dominates the spectrum of the CANFIC perovskite with 1% In, while the original feature at 299.9 cm^{-1} becomes completely suppressed (Fig. 3c, 99.0% Fe). These spectral data, along with the above-discussed XRD results, clearly indicate that the presence of tiny amounts of In(III) in the precursor mixture forwards the reaction toward the formation of cubic CANFIC perovskites with 1% In being enough for the total suppression of the formation of other possible products.

Dried In-free CANFC powder shows a continuous absorption band with an edge at *ca.* 620 nm (Fig. 4a, curve 1). Introduction
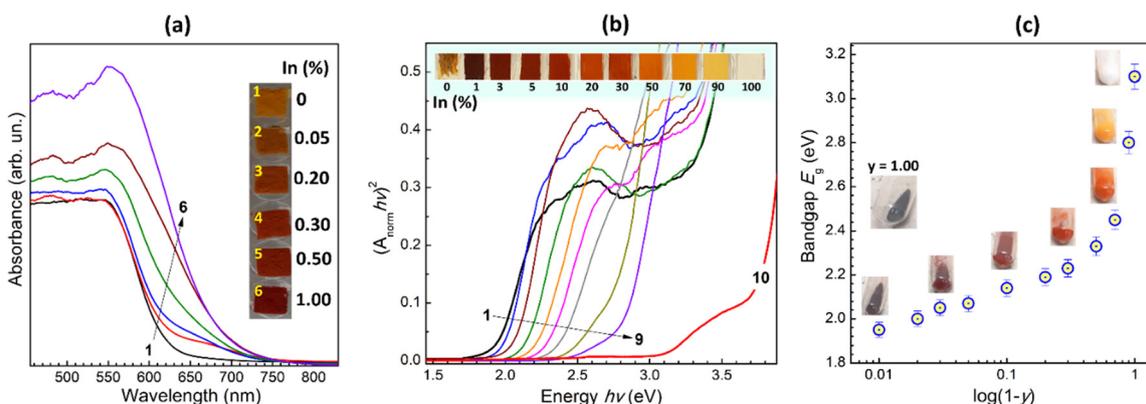

Fig. 4 (a and b) Absorption spectra of CANFICs produced at different nominal Fe fractions. In (a) Fe content in 100% (curve 1), 99.95% (2), 99.8% (3), 99.7% (4), 99.5% (5), and 99.0% (6). In (b) $y = 0.99$ (curve 1), 0.97 (2), 0.95 (3), 0.90 (4), 0.80 (5), 0.70 (6), 0.50 (7), 0.30 (8), 0.10 (9), and 0 (10). Insets in (a and b) show photographs of corresponding dried microcrystalline films on glass. (c) Bandgap E_g of CANFICs as a function of In fraction $(1 - y)$. Insets show photographs of corresponding powders precipitated from 2-propanol in plastic vials.

This journal is © The Royal Society of Chemistry 2023

J. Mater. Chem. C, 2023, **11**, 6867–6873 | **6871**

of even tiny amounts of In, 0.05–0.2%, results in the rise of an additional "shoulder" at longer wavelengths (curves 2 and 3), indicating the formation of an additional CANFIC phase, in agreement with the above-discussed XRD and Raman results. At higher In contents, 0.5–1.0%, this shoulder evolves into a continuous band with the edge at *ca.* 700 nm (Fig. 4a, curves 5 and 6), indicative of the new CANFIC phase dominating the absorption spectrum in such samples.

The absorption spectra of CANFIC perovskites show a distinct linear band edge when plotted in the coordinates of the Tauc equation for direct allowed electron transitions (Fig. 4b), which can be used to estimate direct bandgap from the slope of the linear section of the band edge. Transformation of absorption spectra in the Tauc coordinates for indirect transitions typically results in broadened and strongly non-linear band edges (see an exemplary set of spectra for 1% In in ESI,† Fig. S7), introducing a large uncertainty into the bandgap determination. For this reason, direct bandgaps were adopted in the present report to characterize the evolution of spectral properties of CANFIC perovskites with varied compositions.

As recently reported,[17] both direct and indirect bandgaps of $Cs_2AgFe_xIn_{1-x}Cl_6$ single crystals follow the same trend at the variation of Fe-to-In ratio, indicating that any conclusions on the character of composition-dependent changes of the absorption band edge position can be decoupled from the discussion on the exact nature of the transitions dominating the band edge.

The direct bandgap E_g estimated from the tangent to the linear edge of the absorption spectrum of the CANFIC perovskite with 1% In was found to be 1.95 eV, that is, lower than for pure CANFC product (2.06 eV), and quite close to the bandgap of 1.88 eV reported for iron-pure $Cs_2Ag_{0.58}Na_{0.42}FeCl_6$ perovskite single crystals.[14]

An increase in the In content resulted in a shift of the absorption band edge toward higher energies, without any significant changes in the shape of the band (Fig. 4b). At that, the CANFIC samples change color from deep-brown to brown to orange to yellow, and finally to white for the iron-free CANIC perovskite (inset in Fig. 4b).

Given this "blue" shift induced by further incorporation of In, the CANFIC perovskite with 1% In shows the lowest bandgap of all studied samples, being lower than for Fe-only products and, much lower than for In-only perovskite. The interpretation of the origins of this specific band-bowing behavior requires a separate dedicated investigation. It should also be noted that all In-incorporated perovskites revealed much higher stability toward environmental factors. In particular, the pure-Fe product drop-cast as a microcrystalline film from a suspension in 2-propanol on a glass plate and kept at relative humidity of 50% and higher starts to show signs of hydrolytic decomposition in a few minutes after the solvent evaporation (see the leftmost photograph in Fig. 4b), while the In-containing samples retain perfect stability for many weeks of the shelf-storage in the same conditions.

The dependence of the bandgap of CANFIC perovskites on the Fe-to-In ratio shows two distinct regimes (Fig. 4c). At relatively low In contents corresponding to $y = 0.99–0.50$, the bandgap relatively slowly increases with increasing y from 1.95 eV for $y = 0.99$ to 2.33 eV for $y = 0.50$. Then, at higher In contents, the bandgap increases steeply reaching 2.80 eV for $y = 0.10$ and 3.10 eV for pure CANIC perovskite ($y = 0$).

From these observations, it can be concluded that the incorporation of small Fe admixtures into pure CANIC perovskite exerts a similarly strong impact on the bandgap as the incorporation of small In admixtures into pure CANFC. In particular, the bandgap decrement observed after a mere 10% Fe was incorporated into CANIC (0.30 eV) is almost the same as the total bandgap variation in the much broader range 50–99% Fe (0.38 eV). Such effects of small amounts of metal dopants are typical for double halide perovskites and reported for many compositions, for example, $Cs_2Ag_xNa_{1-x}Bi_yIn_{1-y}Cl_6$.[3,5,12]

Along with the variations of the Fe-to-In ratio, the bandgap of CANFIC perovskites can be tuned to a certain extent by the Ag-to-Na ratio. An increase of the nominal Ag fraction x was found to result in a "red" shift of the absorption edge of CANFIC perovskites with no significant changes in the band shape (ESI,† Fig. S8a). As noted, CANFIC perovskites are formed in a limited range of $0.1–0.2 < x < 0.6–0.7$, while other phases (mixtures of phases) are observed outside this range. In this compositional domain both sets of bandgaps overlap and form an almost linear dependence on the actual Ag content x_a (ESI,† Fig. S8b) with E_g changing from 1.95 eV for $x_a = 0.50$ to 2.28 eV for $x_a = 0.12$.

In conclusion, a series of stable double $Cs_2Ag_xNa_{1-x}Fe_yIn_{1-y}Cl_6$ (CANFIC) perovskites with varied Fe-to-In and Ag-to-Na ratios was produced *via* precipitation at RT and air-open atmosphere. Separation of M^{3+} (Fe and In) and M^+ (Cs, Ag, Na) components in two separate precursors as well as suppression of hydrolytic processes in precursors, by adding concentrated HCl for M^{3+} and ammonia for Ag^+, allows CANFICs to be precipitated as a single product avoiding the formation of secondary phases. The synthetic approach can be scaled to gram quantities and shows a high reproducibility of the structure and spectral properties of the products.

Even a tiny amount of In(III), 0.5–1.0% of Fe content, was found to steer the precursor interaction exclusively towards the formation of environmentally stable solid-solution CANFIC perovskites, while pure CANFC was found to be a mixture of different phases prone to rapid hydrolytic decomposition. Both Fe-to-In and Ag-to-Na ratios in CANFIC perovskites can be controlled in certain ranges by varying nominal x and y parameters at the synthesis.

CANFIC perovskites revealed continuous absorption bands in the visible spectral range with direct bandgaps changing in a broad range by variations of both Fe-to-In and by Ag-to-Na ratios. The lowest bandgap of 1.95 eV (635 nm) was detected for CANFIC perovskite with 1% In ($y_a = 0.99$, $x_a = 0.62$).

A combination of the open-atmosphere character and scalability of the synthetic approach, reliable control over the composition of CANFIC products, the non-toxic and abundant character of constituent elements, and the environmental stability and sensitivity of CANFICs to the visible light down to 1.95 eV makes these perovskites highly promising for

6872 | *J. Mater. Chem. C*, 2023, **11**, 6867–6873

This journal is © The Royal Society of Chemistry 2023

photovoltaic and photochemical applications. Microcrystalline CANFICs can potentially be used as precursors for the formation of thin transparent films for these applications directly by using thermal single-source evaporation as recently shown for similar $Cs_2Ag_xNa_{1-x}Bi_yIn_{1-y}Cl_6$ perovskites[23] or indirectly by preparing CANFIC inks using a solvent-assisted mechano-chemical treatment.

Author contributions

O. Stroyuk: conceptualization (lead), investigation (equal), writing – original draft preparation (lead); O. Raievska: investigation (lead), methodology (lead); A. Barabash: investigation (equal), writing – review & editing (equal); J. Hauch: conceptualization (equal), project administration (lead), writing – review & editing (equal); C. J. Brabec: conceptualization (equal), funding acquisition (lead), writing – review & editing (equal).

Conflicts of interest

There are no conflicts to declare.

Acknowledgements

Notes and references

1 N. K. Tailor, S. Kar, P. Mishra, A. These, C. Kupfer, H. Hu, M. Awais, M. Saidaminov, M. I. Dar, C. Brabec and S. Satapathi, *ACS Mater. Lett.*, 2021, **3**, 1025–1080.
2 W. Ning and F. Gao, *Adv. Mater.*, 2019, 1900326.
3 Y. Liu, A. Nag, L. Manna and Z. Xia, *Angew. Chem., Int. Ed.*, 2021, **60**, 11592–11603.
4 Y. Gao, Y. Pan, F. Zhou, G. Niu and C. Yan, *J. Mater. Chem. A*, 2021, **9**, 11931–11943.
5 O. Stroyuk, O. Raievska, J. Hauch and C. J. Brabec, *Angew. Chem., Int. Ed.*, 2023, **62**, e202212668.
6 F. Ji, G. Boschloo, F. Wang and F. Gao, *Sol. RRL*, 2023, 220112.
7 R. Wang, T. Huang, J. Xue, J. Tong, K. Zhu and Y. Yang, *Nat. Photonics*, 2021, **15**, 411–425.
8 N. K. Tailor, S. Kar, P. Mishra, A. These, C. Kupfer, H. Hu, M. Awais, M. Saidaminov, M. I. Dar, C. Brabec and S. Satapathi, *ACS Mater. Lett.*, 2021, **3**, 1025–1080.
9 M. G. Ju, M. Chen, Y. Zhou, J. Dai, L. Ma, N. P. Padture and X. C. Zeng, *Joule*, 2018, **2**, 1231–1241.
10 J. Liu, J. Qu, T. Kirchartz and J. Song, *J. Mater. Chem. A*, 2021, **9**, 20919–20940.
11 K. Ren, S. Yue, C. Li, Z. Fang, K. A. M. Gasem, J. Leszczynski, S. Qu, Z. Wang and M. Fan, *J. Mater. Chem. A*, 2022, **10**, 407–429.
12 O. Stroyuk, O. Raievska, A. Barabash, C. Kupfer, A. Osvet, V. Dzhagan, D. R. T. Zahn, J. Hauch and C. J. Brabec, *Mater. Adv.*, 2022, **3**, 7894–7903.
13 W. Li, N. U. Rahman, Y. Xian, H. Yin, Y. Bao, Y. Long, S. Yuan, Y. Zhang, Y. Yuan and J. Fan, *J. Semicond.*, 2021, **42**, 072202.
14 Y. Xian, H. Yin, Y. Bao, Y. Xiao, S. Yuan, N. U. Rahman, Y. Yuan, Y. Zhang, X. Meng, S. Jin, W. Li and J. Fan, *J. Phys. Chem. Lett.*, 2020, **11**, 9535–9542.
15 P. Han, C. Luo, W. Zhou, J. Hou, C. Li, D. Zheng and K. Han, *J. Phys. Chem. C*, 2021, **125**, 11743–11749.
16 H. Yin, Y. Xian, Y. Zhang, W. Chen, X. Wen, N. U. Rahman, Y. Long, B. Jia, J. Fan and W. Li, *Adv. Funct. Mater.*, 2020, **30**, 2002225.
17 F. Ji, F. Wang, L. Kobera, S. Abbrent, J. Brus, W. Ning and F. Gao, *Chem. Sci.*, 2021, **12**, 1730–1735.
18 R. Udavant, S. Thawarkar, S. Rondiya, A. Shelke, R. Aher, T. G. Ajithkumar, R. W. Cross, N. Y. Dzade and S. Jadkar, *Inorg. Chem.*, 2023, **62**, 4861–4871.
19 D. Manna, J. Kangsabanik, T. K. Das, D. Das, A. Alam and A. Yella, *J. Phys. Chem. Lett.*, 2020, **11**, 2113.
20 A. C. Dakshinamurthy and C. Sudakar, *J. Phys. Chem. Lett.*, 2022, **13**, 433.
21 G. A. Voyiatzis, A. G. Kalampounias and G. N. Papatheodorou, *Phys. Chem. Chem. Phys.*, 1999, **1**, 4797–4803.
22 B. Zhang, J. Klarbring, F. Ji, S. I. Simak, I. A. Abrikosov, F. Gao, G. Y. Rudko, W. M. Chen and I. A. Buyanova, *J. Phys. Chem. C*, 2023, **127**, 1908–1916.
23 O. Stroyuk, O. Raievska, P. Sebastia-Luna, B. A. H. Huisman, C. Kupfer, A. Barabash, J. Hauch, H. J. Bolink and C. J. Brabec, *ACS Mater. Lett.*, 2023, **5**, 595–602.

This journal is © The Royal Society of Chemistry 2023

J. Mater. Chem. C, 2023, **11**, 6867–6873 | **6873**